https://doi.org/10.5194/egusphere-2025-5364
Preprint. Discussion started: 18 December 2025

TerraceM-3: Integrating machine learning and ICESat-2 altimetry to estimate deformation rates from wave-abrasion terraces

Julius Jara-Muñoz[1], Jürgen Mey[2], Roland Freisleben[3], Daniel Melnick[4], Markus Weiss[8], Patricio Winckler[5,6,7], Chrystelle Mavoungou[8], Manfred R. Strecker[3]

[1]Institute of Earth and Environmental Sciences, Faculty of Civil Engineering, Biberach University of Applied Sciences, Germany
[2]Institute of Environmental Science and Geography, University of Potsdam, Germany
[3]Institute of Geosciences, University of Potsdam, Germany
[4]Instituto de Ciencias de la Tierra, Universidad Austral de Chile, Valdivia, Chile
[5]Escuela de Ingeniería Oceánica, Universidad de Valparaíso, Chile
[6]Centro de Investigación Para La Gestión Integrada del Riesgo de Desastres (CIGIDEN), Chile
[7]Centro de Observación Marino Para Estudios de Riesgos del Ambiente Costero (COSTAR), Chile
[8] Institute of Applied Biotechnology, Biberach University of Applied Sciences, Germany

Correspondence: Julius Jara-Muñoz (jara@hochschule-bc.de)

https://doi.org/10.5194/egusphere-2025-5364
Preprint. Discussion started: 18 December 2025

Abstract

Wave-abrasion terraces are geomorphic marker horizons that provide information of past water levels, in marine and lacustrine environments. By integrating elevation measurements and age knowledge they serve as strain markers to assess vertical deformation rates associated with tectonic and/or climatic processes. As most geomorphic markers, wave-abrasion terraces are ephemeral features, and their topographic signature has variable levels of noise. Therefore, accurate and precise estimates of marine terrace morphology are essential to obtain significant uplift/subsidence rates. TerraceM-3 enables users to reduce non-systematic and systematic errors in terrace mapping by integrating machine learning techniques to replicate human mapping criteria, and standardized and reproducible workflows to handle systematic errors. In many regions, the availability of high-resolution topographic data remains relatively scarce limiting precision in geomorphic marker mapping. TerraceM-3 introduces a new module for downloading, filtering, and processing centimeter-resolution topographic data from the ICESat-2 satellite at global scale. The TerraceM-ICESat module produces vegetation-free profiles ready for assisted machine-learning mapping into a graphical user interface. Shallow bathymetry may be also extracted to extend the mapping of drowned terraces offshore. The new functionalities of TerraceM-3 were tested along tectonically active coasts in Peru and Algeria, revealing detailed deformation histories controlled by subducted seamounts and crustal faults. TerraceM-3 is designed to support research in tectonic geomorphology and paleoclimate studies by enhancing the precision and accuracy of wave-abrasion terrace mapping with applications in the assessment of coastal hazards.

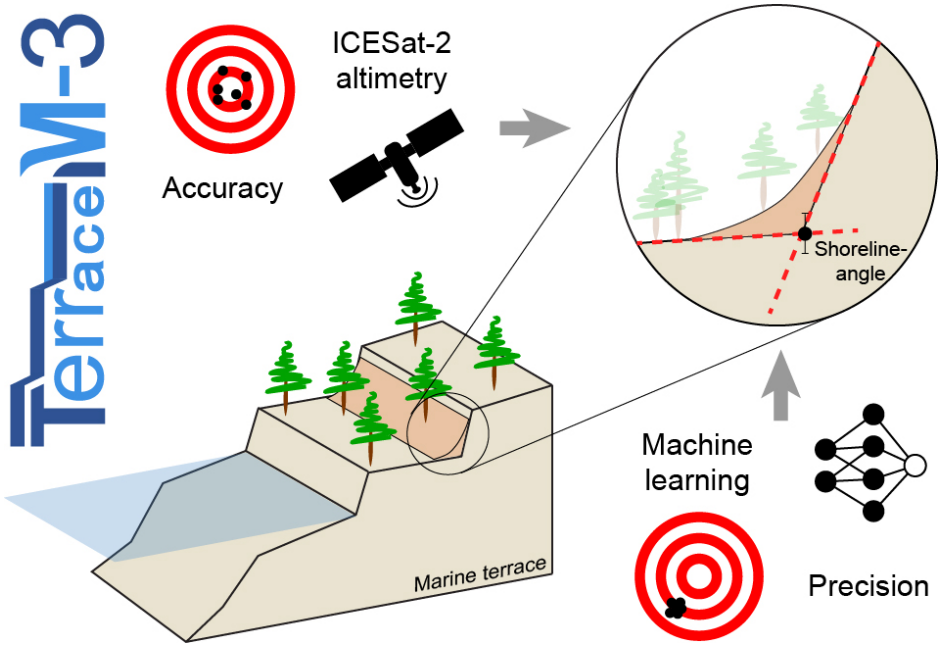

Graphical abstract

https://doi.org/10.5194/egusphere-2025-5364
Preprint. Discussion started: 18 December 2025

1. Introduction

Coastal areas are highly vulnerable to natural hazards such as sea-level rise, earthquakes, and tsunamis. Understanding past changes in coastal environments, requires accurate measurements of surface deformation, which are fundamental for elucidating the governing mechanisms within the solid Earth. This is particularly relevant over millennial timescales, when the interplay between multiple geodynamic and climatic processes needs to be disentangled for proper interpretation. Precise measurements of vertical deformation at these time-scales are essential for distinguishing among various driving mechanisms and their temporal evolution, including tectonic forces from plate boundary interactions, glacial isostatic adjustment following ice-sheet retreat and magmatic inflation (e.g. Lambeck, 2001; Pan et al., 2021; Singer et al., 2018; Fialko and Pearse, 2012; Simms et al., 2016). Furthermore, quantifying rates associated with these processes at centennial to millennial scales is necessary to separate these long-term natural processes from land-level changes driven by modern anthropogenic activities such as groundwater withdrawal hydrocarbon extraction (e.g. Geertsma, 1973; Holzer and Johnson, 1985; Shirzaei et al., 2021). In coastal areas, the records of deformation at millennial scales can be preserved as fossil geomorphic features in the landscape, such as marine or fluvial terraces, and as fault scarps or offsets. Nevertheless, their ephemeral nature makes difficult the direct estimation of deformation rates from surface morphology (e.g. Anderson et al., 1999).

Wave-abrasion marine terraces have been largely used to estimate vertical deformation rates (Lajoie, 1986; Pedoja et al., 2011; Kaizuka et al., 1973). These geomorphic features are formed by wave abrasion during past sea-level positions, representing fossil markers of deformation that can extend by several kilometers along the coast. Marine terraces are often exposed forming sequences of several terraces that record past sea-level variability at glacial cycle time-scales. These special characteristics make marine terraces valuable for estimating past sea-level positions and the temporal and spatial distribution of deformation (Burbank and Anderson, 2011; Anderson et al., 1999; Chappell, 1974; Roberts et al., 2013; Lajoie, 1986; Broecker et al., 1968; Armijo et al., 1996). As such, marine terraces and their equivalents in the lacustrine realm are first-order geomorphic strain markers that furnish primary observational constraints for understanding the rheological structure of the lithosphere, active deformation of plate boundaries and the mechanical behavior of active fault systems (e.g. Henriquet et al., 2019; Simms et al., 2016; Armijo et al., 1996; Sato and Matsu'ura, 1992; Ghazleh and Kempe, 2009; Jara-Muñoz et al., 2024; Ghazleh and Kempe, 2021). However, despite its extensive application, mapping marine terraces has traditionally been a qualitative process, often relying on subjective criteria, which has direct repercussions regarding the precision and accuracy of these markers. In addition, topographic datasets used for marine terrace mapping can include further errors related to data acquisition, topographic artifacts, vegetation, and poor spatial resolution. Such errors can lead to misinterpretations of the underlying deformation processes, particularly when attempting to identify low magnitude deformation rates of over hundreds of thousands to millions of years (e.g. Melnick, 2016; Regard et al., 2010).

https://doi.org/10.5194/egusphere-2025-5364
Preprint. Discussion started: 18 December 2025

1.1 Marine terrace mapping: methods and uncertainties

While several studies have proposed useful methods to map marine terraces using high-resolution topography (Bowles and Cowgill, 2012; Jara-Muñoz et al., 2019; Jara-Muñoz et al., 2016; Palamara et al., 2007), the accuracy of these measurements can be significantly compromised by processes that destroy or alter the marine terrace morphology (Fig. 1A-H). For instance, river erosion (Fig. 1B) can effectively destroy the original marine terrace morphology by retreat of slopes adjacent to incising streams (Anderson et al., 1999; Rosenbloom and Anderson, 1994). Diffusion of material from paleo-cliffs and landslides (Fig. 1C-D) can modify the cliff edge and the original slope of both, paleo-cliff and paleo-platform (Hanks et al., 1984; Stephenson, 2015; Griggs and Trenhaile, 1994). Marine terrace deposits, such as alluvial cover, coastal sediments, and active dunes (Fig. 1E), may cover the paleo-platform, potentially leading to overestimation of terrace elevation (Jara-Muñoz and Melnick, 2015).

Rough coasts along rocky shorelines, formed under intense wave erosion and high bedrock erodibility or affected by strong weathering or bioerosion, result in the formation of sea-stacks and stumps above the paleo-platform (Fig. 1F) (Trenhaile et al., 1998). These topographic irregularities may hinder the assessment of the marine terrace morphology (Jara-Muñoz et al., 2016). Furthermore, differential bedrock erosion, particularly at lithological contacts between rocks of varying erodibility, or the effect of river erosion and non-marine processes, can result in the formation of "pseudo terraces" (Duff, 1993; Mitusio, 1989) and thus an erroneous evaluation of terrace levels (Fig. 1G). Additionally, anthropogenic modification of the landscape can significantly alter terrace morphology (Fig. 1H). For instance, marine terraces are frequently used for the construction of roads and urban centers, often involving slope reshaping and infilling of the paleo-platform, complicating the mapping of marine terrace elevations. Finally, the low-resolution of digital topography, may compromise the assessment of terrace morphology (Fig. 1I) by smoothing out natural terrain slopes (Chang and Tsai, 1991).

One of the main challenges when mapping marine terraces is the limited availability of high-resolution digital topography (0.5 - 5 m/pixel), currently restricted to certain countries and isolated areas such as those accessible through the OpenTopography portal (Krishnan et al., 2011). Furthermore, the resolution and accuracy of the available medium-resolution digital topography (10 - 30 m/pixel) can significantly influence the accuracy of terrace mapping (Jara-Muñoz et al., 2016). Recently, satellite altimetry missions such as NASA's ICESat-2 have provided highly accurate bare-earth elevation data (Abdalati et al., 2010; Markus et al., 2017; Jasinski et al., 2021). Unlike traditional gridded digital elevation models (DEMs), ICESat-2 uses photon-counting LiDAR to capture high-resolution elevation profiles, reducing artifacts and effectively filtering out vegetation (Neuenschwander and Pitts, 2019).

https://doi.org/10.5194/egusphere-2025-5364
Preprint. Discussion started: 18 December 2025

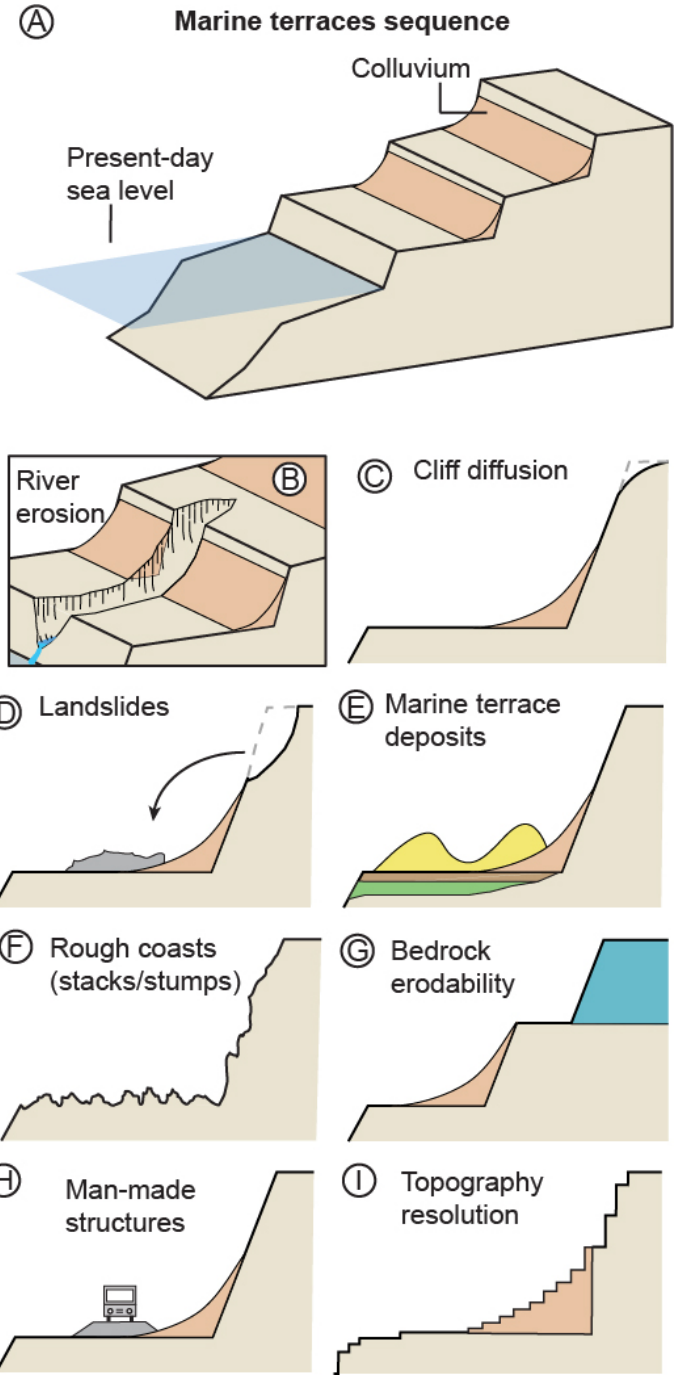

Figure 1: Processes and environmental factors affecting the morphology of wave-abrasion marine terraces. A) Simplified anatomy of a marine terrace sequence. B-I) Examples of processes and factors that can alter or destroy the marine terrace topography compromising their identification and mapping.

https://doi.org/10.5194/egusphere-2025-5364
Preprint. Discussion started: 18 December 2025

1.2 The TerraceM project

Since its first release, TerraceM has included methods to mitigate the effects of river erosion and cliff diffusion when mapping marine terrace elevations by using swath topographic profiles (Fig. 2A-D, Jara-Muñoz et al., (2019; 2016)). However, the influence of processes that destroy marine terrace morphology remains difficult to discriminate using digital topography and often requires calibration through field observations and detailed geomorphic interpretations (e.g. Matsu'ura et al., 2014; Matsu'ura, 2015; Melnick et al., 2017; Bowles and Cowgill, 2012; Matsu'ura et al., 2019; Berryman, 1993). Consequently, terrace identification and mapping remain partly dependent on the operator's criteria. The TerraceM mapping approach requires the operator to manually define two segments along a topographic profile (Jara-Muñoz et al., 2019; Jara-Muñoz et al., 2016), a couplet comprising the paleo-platform and paleo-cliff of a wave-abrasion marine terrace (Fig. 2C). Linear regressions are then fitted to both segments and extrapolated (Fig. 2D); their intersection defines the shoreline-angle, which represents the marine terrace elevation (Fig. 2D) and which marks the former water level during marine or lacustrine highstands (Lajoie, 1986). The shoreline-angle elevation error is derived from the confidence interval of the linear regressions.

The shoreline-angle mapping procedure involves a degree of subjectivity, as the manual placement of paleo-cliff and paleo-platform segments can vary depending on operator criteria such as complex decision processes and experience. Based on data collected during experiments with different users, Jara-Muñoz et al. (2016) proposed that terrace mapping can be a repeatable process within a certain degree of confidence, although it still depends on subjective interpretation and user experience (non-systematic errors). The advancement of artificial intelligence and machine learning methods combined with the increasing computational power of desktop computers has made it possible to analyze and reproduce complex, non-linear relationships involving a wide range of variables. These include user-based decisions and the qualitative criteria inherent to human-machine interactions (e.g. Johannsen, 2009; Schleidgen et al., 2023). Applying machine learning to automate marine terrace mapping offers the potential to address the qualitative nature of traditional approaches and reduce the non-systematic errors associated with human interpretation.

TerraceM is an open-source software written in MATLAB® and originally designed for measuring marine terraces systematically using swath profiles and estimating surface deformation rates (Jara-Muñoz et al., 2016). In the subsequent versions, TerraceM-2 incorporated numerical models to simulate marine terrace formation and to analyze deformation patterns produced by active faults and deep deformation sources (Jara-Muñoz et al., 2019). In the present release, TerraceM-3 introduces a new automatic marine terrace mapping module powered by machine learning (ML) algorithms, along with an integrated interface for directly downloading, processing, and mapping marine terraces using high-resolution satellite altimetry data of the ICESat-2 mission (Fig. 3). TerraceM-3 also includes TerraceM PreMAP, a novel workflow to improve the accuracy of marine terrace mapping by systematizing the preparation of swath profiles (Fig. 3). We applied these new approaches at

https://doi.org/10.5194/egusphere-2025-5364
Preprint. Discussion started: 18 December 2025

Cerro El Huevo, Peru, and Sahel Ridge, Algeria, obtaining accurate and precise deformation estimates that reveal detailed tectonic deformation histories and the influence of deep deformation sources and crustal faults.

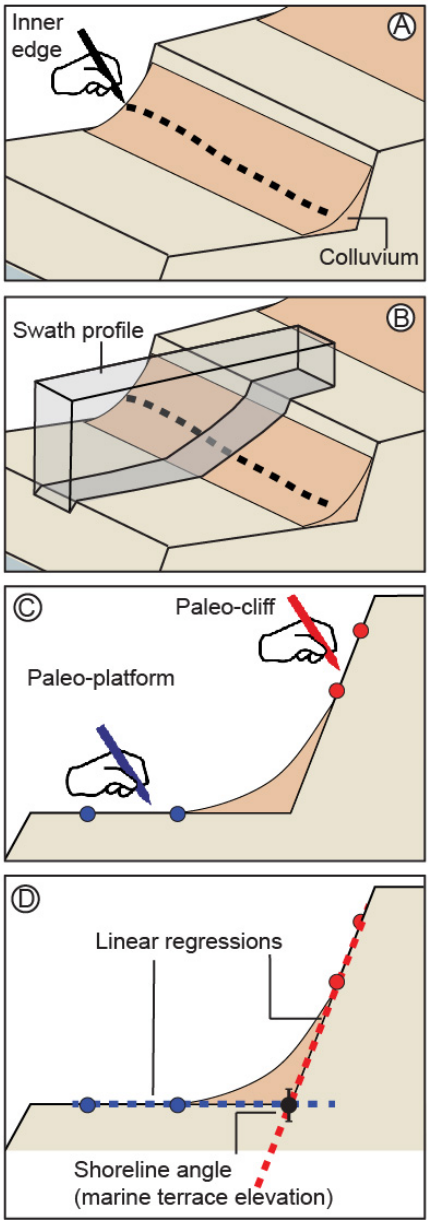

Figure 2: The classical TerraceM workflow (Jara-Muñoz et al., 2016) includes: a) manual mapping of inner edges in a GIS platform; b) placement of swath profiles perpendicular to inner edge and check profile locations c) manual mapping of paleo-cliff and paleo-platform segments in the swath profile; and d) extrapolation of linear regressions from the topography segments. The intersection of these regressions defines the shoreline angle, which represents the marine terrace elevation.

https://doi.org/10.5194/egusphere-2025-5364
Preprint. Discussion started: 18 December 2025

2. New methodological approaches in TerraceM-3

2.1 Systematic approaches in the TerraceM_PreMAP module

Systematic approaches are essential for obtaining reproducible and accurate measurements. By following a systematic approach, a workflow can be designed to include unambiguous steps, standardized methods, data quality control, and reproducibility protocols yielding reliable and consistent outcomes (Atkinson et al., 2017). The classical TerraceM mapping workflow consists of four main steps (Fig. 2A-C) (Jara-Muñoz et al., 2019; Jara-Muñoz et al., 2016): (1) preliminary mapping of the inner edges of marine terraces, identified at the slope break between the paleo-platform and paleo-cliff, within a Geographic Information System (GIS; e.g., QGIS®, Fig. 2A); (2) placement of swath-profile boxes perpendicular to the inner edges and verification of their positioning (Fig. 2B); the boxes are preferably located in areas with optimal terrace exposure, avoiding valleys, anthropogenic structures, and landslides; and (3) manual mapping of marine terraces along swath profiles (Fig. 2C). The mapping focuses on the shoreline angle, a geomorphic marker that represents the relative sea-level elevation at the time of marine terrace formation (Jara-Muñoz et al., 2016; Lajoie, 1986). Thus, shoreline-angle measurements refer to the measurement of the elevation of the intersection between the platform and the cliff, rather than to the angle itself. Although this mapping procedure follows logical steps and standardized criteria, certain aspects remain challenging to produce consistent outcomes, potentially leading to systematic errors.

The first step of the classical TerraceM workflow is the inner edge mapping (Fig. 2A), which can be straightforward if the mapper has a basic knowledge on the morphology of marine terraces and GIS software. Usually, a slope model combined with an elevation colormap can help identifying the approximate position of the inner edges (Palamara et al., 2007), or a red relief image (RRIM, provided as a QGIS toolbox on www.terracem.com) that highlights subtle changes in slope, and terrain openness (Chiba et al., 2008). A common issue when mapping the inner edge arises from the erroneous assignment to a terrace level, especially when age constraints are scarce. For example, in areas of intense coastal erosion and river incision, marine terrace exposures might be discontinuous, which can complicate the lateral correlation of terrace levels in the topography (e.g. Johnson, 1944; Cerrone et al., 2021). This is an important aspect, as the miscorrelation between marine terrace levels can affect the correspondence of shoreline-angle measurements to a specific sea-level position in the past and hence the estimated uplift rates.

To address these challenges, TerraceM-3 includes the module TerraceM_PreMAP (Fig. 3) that follows a systematic approach for checking and correcting the inner edge mapping process and lateral correlations. The module enables comparison between the mapped inner edges and an innovative variant of topographic profile display defined as ‘Stacked Swath’, which is based on stacked parallel profiles (De Gelder et al., 2022; Curveur, 2012; Armijo et al., 2015; Forte and Whipple, 2019). The stacked swath forms a structured 2D point cloud in distance-elevation space, where each point corresponds to a topographic measurement (Forte and Whipple, 2019). This approach enables the identification of low-slope areas (e.g., paleo-platforms)

https://doi.org/10.5194/egusphere-2025-5364
Preprint. Discussion started: 18 December 2025

through increased point density and highlights zones of sharp slope change, such as at inner edge locations, along the coastal transect (See further information on Supplementary material Section S1, figures S1 to S7).

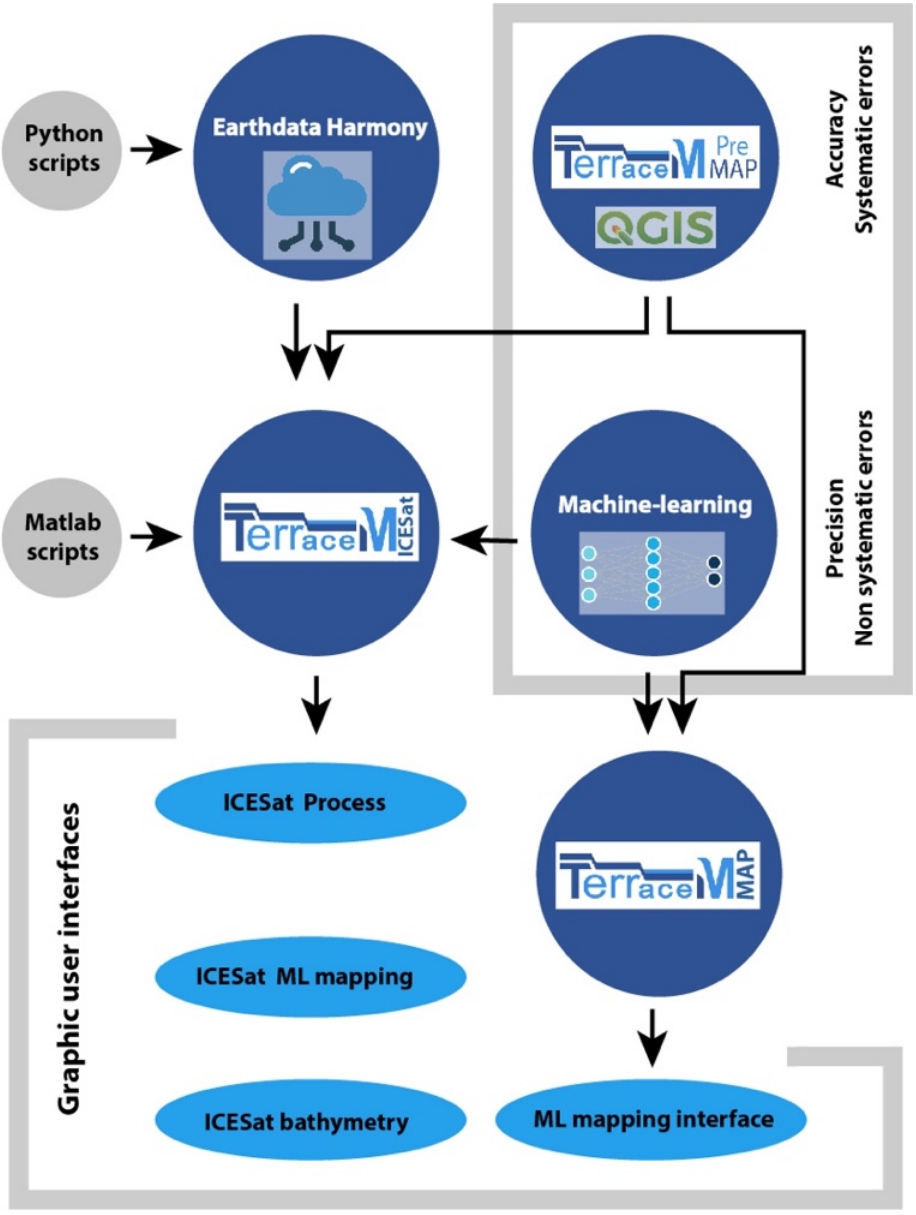

Figure 3: Architecture of TerraceM-3 and its new modules. TerraceM-3 includes three modules (TerraceM_ICESat-2, TerraceM_PreMAP, and TerraceM_MAP) and two functions for integration with Earthdata Harmony (NASA) and machine learning. TerraceM_PreMAP and the machine-learning function are designed to reduce systematic and non-systematic errors, feeding into TerraceM_ICESat-2 and MAP. TerraceM_ICESat-2 is powered by Python scripts running into MATLAB®, and both ICESat and MAP provide graphical user interfaces in MATLAB® that enable efficient application of the methods. TerraceM_MAP was originally release in TerraceM-2 and updated with machine learning in this version.

https://doi.org/10.5194/egusphere-2025-5364
Preprint. Discussion started: 18 December 2025

2.1.1 Increasing resolution of marine terrace mapping with TerraceM_PreMap at Cerro El Huevo

We tested TerraceM_PreMAP at Cerro El Huevo (Figs. 4A–4C) on the Peruvian convergent margin, a site characterized by remarkably well-preserved and well-studied marine terraces (Hsu, 1988; Ortlieb and Macharé, 1990; Saillard et al., 2011; Hsu, 1992). In addition, the area is located in a complex geodynamic setting, making it an ideal scenario for testing the TerraceM_PreMAP approach. In southern Peru the Nazca plate subducts obliquely (N79°E) beneath South American plate at 68 – 77 mm/yr (Demets et al., 1990; Norabuena et al., 1998). This sector of the margin also involves the ongoing subduction of the Nazca Ridge (NR, Figs. 4A and B), which began near Ecuador ~40 Ma and has since migrated southward (Bello-González et al., 2018). The marine terraces sequence at Cerro El Huevo consist of eight levels reaching ~200 m asl that were deformed by the subduction of the NR (Fig 4C) (Jara-Muñoz et al., 2019; Saillard et al., 2011; Hsu, 1992). The uplift distribution is notably asymmetric relative to the incoming NR bathymetry (Hampel et al., 2004; Hsu, 1992), with the maximum uplift above its leading southern flank (Fig. 4B). As a result of the complex interplay of vertical displacements, eolian sediment transport and erosion, some terrace levels are discontinuous and their lateral continuity is difficult to discern, providing an excellent setting to evaluate our lateral correlation method.

We mapped eight levels of marine terraces using a RRMI derived from the 12-m resolution TanDEM-X topography provided by the Deutsches Zentrum für Luft- und Raumfahrt (DLR). We used the stacked swath to check the lateral continuity of terrace levels along the coastal region (Figs. 4D-E). This procedure corrected previous miscorrelations, such as those between terrace levels 3 and 4, and the discontinuous exposures of levels 7 and 8 below the summit of Cerro El Huevo (Fig. 4D–F). Although the inner edges represent only the maximum estimate of the marine terrace elevation (Jara-Muñoz et al., 2016), we can observe variations of tilt between marine terrace Levels 8 - 5 and 4- 2 (Fig. 4E and 4F). The accurate estimation of tilt angles is based on shoreline angles measured with ML, which are presented in section 2.2.1.

https://doi.org/10.5194/egusphere-2025-5364
Preprint. Discussion started: 18 December 2025

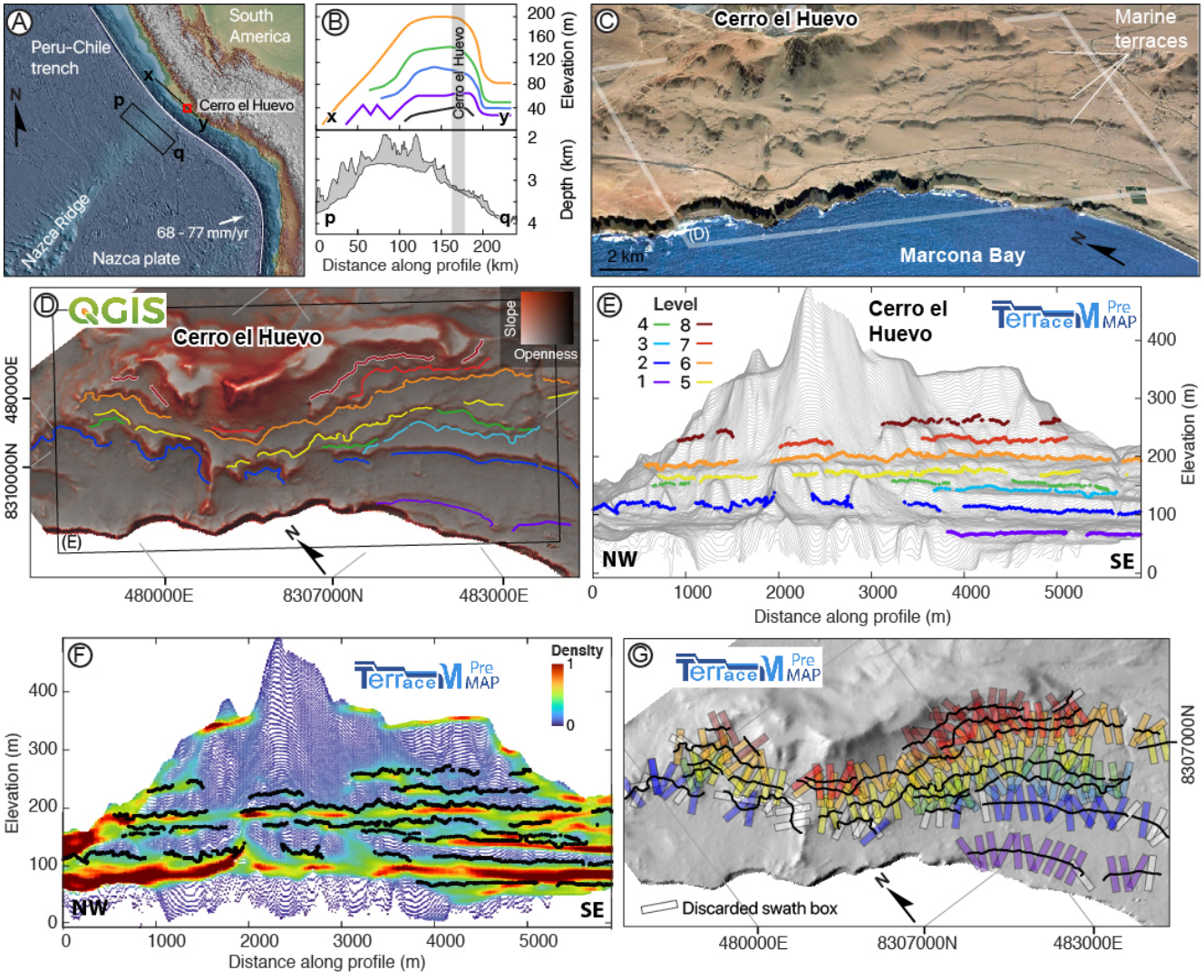

Figure 4: TerraceM_PreMAP workflow at Cerro El Huevo and tectonic context. A) location of Cerro El Huevo and the Nazca Ridge. B) Regional elevation patterns of marine terraces based on Hsu et al. (1992) and bathymetric swath profile of the Nazca Ridge. C) Digital 3D perspective based on Digital Globe® imagery of Cerro El Huevo and Marcona Bay in Southern Peru. D) Inner edge mapping using a RRIM in QGIS. Inner edge colors represent marine terrace levels (legend in E). The black rectangle is the area used for the stacked swath profile. E and F) Joint visualization of inner edges and stacked swath profile, including lines and point density. G) Automated extraction of swath boxes based on inner edges, manually discarded boxes in white. The swath profile boxes are now ready for shoreline-angle mapping.

The variability in swath profile spacing, orientation, width, and length can introduce additional systematic errors in marine terrace mapping and measurement (Jara-Muñoz et al., 2016). To minimize these errors, TerraceM_PreMAP automatically generates swath profile boxes oriented perpendicular to the inner edge trace, with user-defined parameters such as width and spacing (Fig. 4D). Next, the swath boxes are manually revised and those located in valleys or in areas with poor marine terrace

https://doi.org/10.5194/egusphere-2025-5364
Preprint. Discussion started: 18 December 2025

exposure are excluded. The manual exclusion of swath boxes helps eliminate potential mapping errors and increases the precision of marine terrace mapping. For instance, along terrace level 2, of Cerro El Huevo, the stacked swath and the inner edge mapping reveals areas of scattered elevations. This variability reflects the accumulation of colluvial and eolian deposits at the inner edge. Based on these observations, swath boxes in covered areas and valleys were manually excluded (Fig. 4G).

2.2 Automated mapping of marine terraces using neural networks

Supervised ML algorithms, often referred to as "black-box" tools, rely on the training of artificial neural networks (NNs), which have the ability to learn from experience (Tang et al., 2020; Bishop, 1995). A NN consists of multiple layers of interconnected artificial neurons that simulate the way biological neurons process information (Wang, 2003) (Fig. 5A). Neurons of adjacent layers receive and transmit information through a number of weighted connections, which eventually leads to a response of the entire system, the output. Each node is assigned a layer-specific activation function, which takes the weighted sum of the inputs plus a bias and produces the node's response value. These response values represent the inputs to the nodes of the next layer and so on. During the training phase, the network is fed with a number of input-output examples or training data. Through multiple iterations, the network adjusts the weights to minimize the error between the predicted and the observed outputs and learns to recognize complex patterns in the data (e.g. Fig. 5B), improving its predictive accuracy (Wu and Feng, 2018). This recursive learning process continues until a predefined stop-criterion is met, e.g. the number of learning epochs or cycles, or until the algorithm achieves a high level of accuracy and generalization, which shows that the NN has learned correctly.

Because the central property of NN's is their ability to generalize from training data it is essential to obtain a large and representative training dataset. The quality of this dataset is crucial for the NN performance and should be carefully filtered and classified before training (Kavzoglu, 2009). For this purpose, we used the continuous mapping of the last interglacial (MIS 5e) terrace along the coast of South America that comprises ~2000 shoreline-angle measurements (Fig. 5C) (Freisleben et al., 2020). After manual filtering, we split the data, selecting 1000 representative measurements for NN training and removing outliers and noise, while the remaining measurements were subsequently used for validation. The data consisted on distance/elevation data from swath profiles, paleo-cliffs and paleo-platforms and was normalized to a 0–1 scale (See supplementary material 1 for further information). We trained two separate feedforward NNs, one for the paleo-cliff zone and another for the paleo-platform zone. Each NN consisted of three hidden layers with 100 Neurons per layer and used a log-sigmoid activation function (Fig. 5A). Training performance was evaluated using the mean squared error (MSE) and learning gradients, both dimensionless values (Fig. 5B). The MSE is used as loss function that measures the difference between measured and predicted outputs by the NN. The gradients represent the partial derivative of the loss function (MSE) with respect to model parameters and indicates the direction and magnitude of change needed to reduce the error (See additional information provided in Supplementary material Section S2). MSE and gradients decreased progressively as learning progressed. A steep reduction in MSE was observed during the first ~30 epochs, followed by a gradual decline that stabilized

https://doi.org/10.5194/egusphere-2025-5364
Preprint. Discussion started: 18 December 2025

around epoch 600 at MSE values of 0.002. Likewise, the gradient decreased gradually, but interrupted by peaks, whose magnitude and frequency decreased along the training. Most importantly, the overall MSE versus epoch learning curve was smooth and showed a clear trend, indicating efficient training (Fig. 5B).

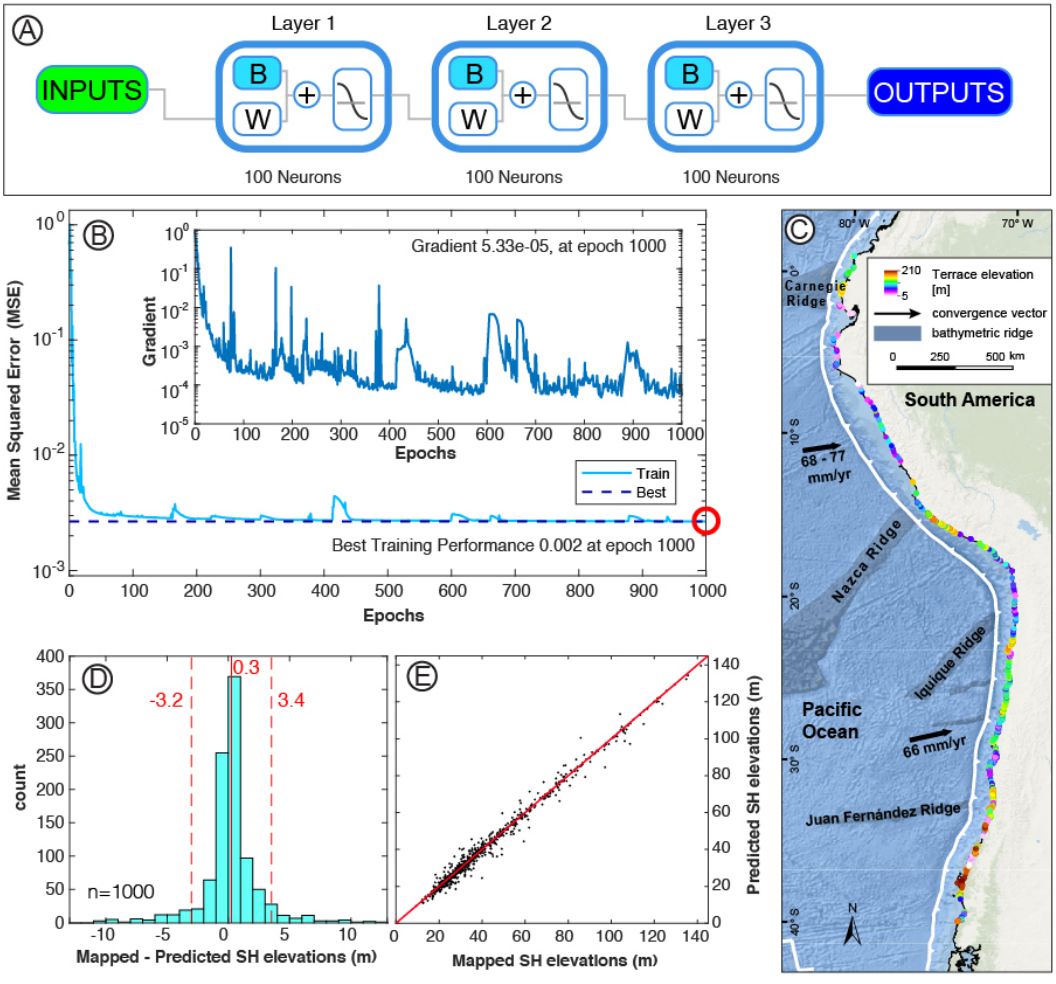

Figure 5: Neural Network architecture, training and testing. A) Neural network (NN) used for the automated recognition of paleo-platform and paleo-cliff segments. B and W represent bias and weights, respectively. The curve represents a sigmoidal function. B) example of NN training showing variations in gradients and mean squared error (MSE); note the smooth decline of MSE and stabilization around epoch 600. C) Training and testing data based on 2000 shoreline-angles mapped along South America (Freisleben et al., 2020). D and E) NN test using the remaining 1000 shoreline-angles not used for NN training.

We tested our trained neural networks using the remaining shoreline angle measurements along the western South American coast that were not used for initial training (Fig. 5D and E). The resulting predictions showed strong agreement with the original manually mapped shoreline angles, with a mean difference of ~0.3 m (Fig. 5D), which is one order of magnitude lower than

https://doi.org/10.5194/egusphere-2025-5364
Preprint. Discussion started: 18 December 2025

the ~2.5 m mean shoreline-angle elevation error of the training data. We implemented the NN into an automated mapping tool in TerraceM MAP module.

2.2.1 Quantifying collision of the Nazca Ridge with automatic mapping

We applied the automated shoreline-angle mapping to our study site at Cerro El Huevo, mapping the swath boxes automatically extracted by TerraceM_PreMAP. For a total number of 200 swath boxes, 26 boxed were excluded due to wrong orientation or placement on covered terrace areas. From the remaining 174 swath boxes 17 could not be mapped by ML due to the small expression of the terraces and insufficient topographic points to extract the linear regressions for shoreline-angle mapping. We obtained between 11 and 34 shoreline angles for each marine terrace level that follow the trace of the inner edges. Based on the dating of marine terraces carried by Saillard et al. (2011) and numerical modeling of marine terraces by Jara-Muñoz et al. (2019) we correlate the marine terrace levels with the interval of highstands between MIS 5c to MIS 13 (Fig. 6A). We extracted linear regressions using the shoreline angles of each terrace level observing a progressive change in the tilt angle and tilt direction. For instance, the older marine terrace levels 8 – 6, displayed a NW tilt direction with angles varying between ~0.5 and ~0.1°. The marine terrace levels 5 – 4 are sub-horizontal, whereas the marine terrace levels 3 -1 showed a SE tilt direction with tilt angles between ~-0.05 and ~-0.4° (Fig. 6B). This change in tilt polarity and magnitude in time is expected to result from changes in surface deformation linked to the subduction of the NR. As indicated in Section 2, the oblique convergence between Nazca and South America plates results in the southward migration of the NR at a velocity of 43 mm/yr (Hampel, 2002). On the other hand, Cerro El Huevo is located south of the indentation point of the NR and at the edge of the deformation bulge produced by the ridge subduction (Fig. 4B). This setting makes Cerro El Huevo a sensible recorder of changes in vertical deformation linked to the position of the NR and its migration along the margin.

https://doi.org/10.5194/egusphere-2025-5364
Preprint. Discussion started: 18 December 2025

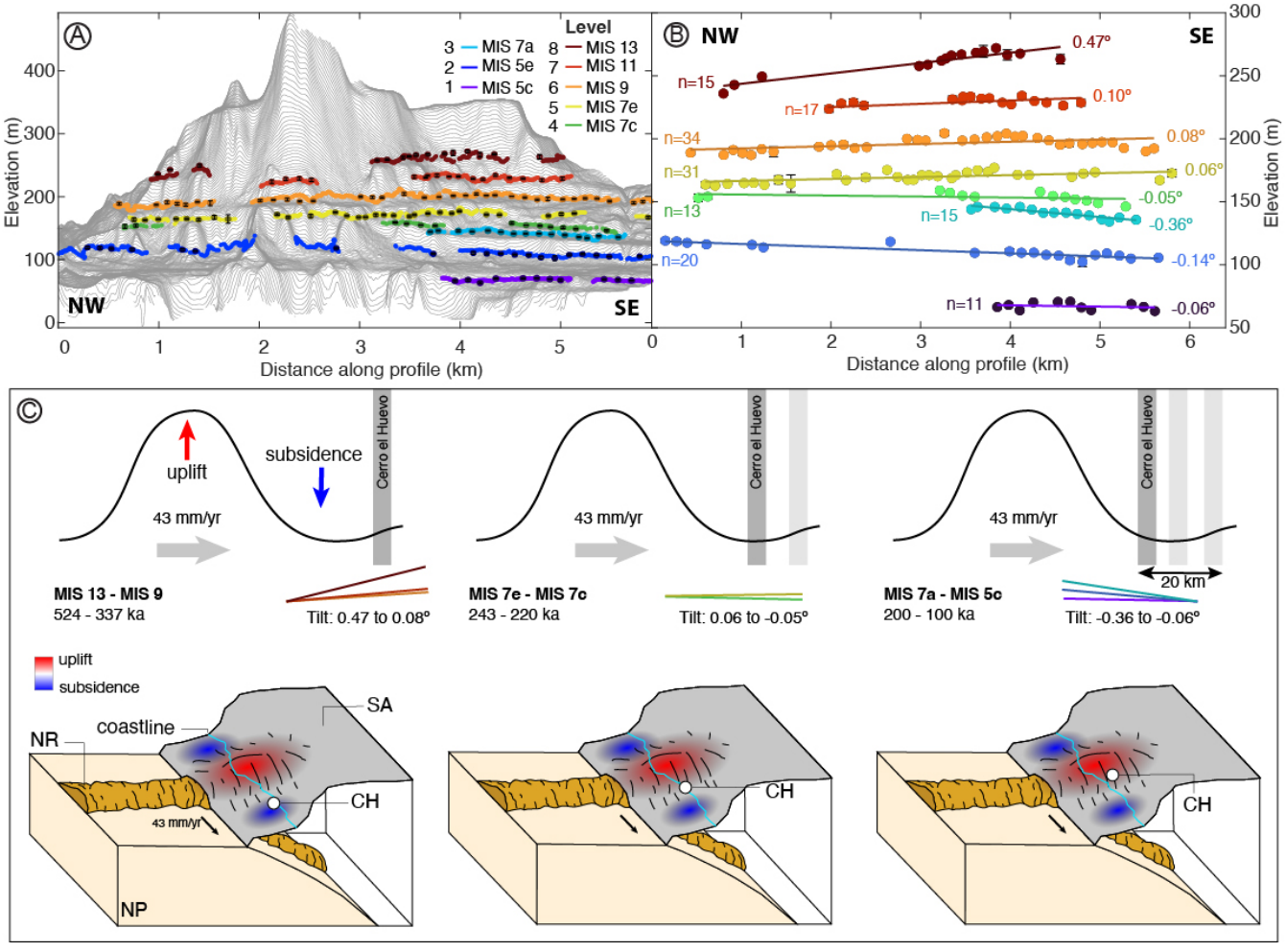

Figure 6: Distribution of shoreline-angle elevations, tilt angles and deformation mechanisms. A) Shoreline-angle mapping overlapping a stacked swath and inner edges. Notice the coherence between inner edge level and shoreline angles. B) Tilt estimates from linear regressions of shoreline angles across marine-terrace levels (n = number of shoreline angles). C) Conceptual model to explain changes in tilt angles: between MIS 13 and 9 Cerro El Huevo (CH) was located at the margin of the subsiding zone (northward tilt); at MIS 7 it was near the hinge between uplift and subsidence (almost no tilt); between MIS 7 and MIS 5c it reached the flank of the uplifting bulge (southward tilt). NR: Nazca Ridge, NP: Nazca plate, SA: South American plate.

Our mapping of marine terraces along the El Huevo coast using TerraceM-3 allows refining and better quantifying rates from the initial conceptual model proposed by Macharé and Ortlieb (1992) and Hsu (1992). In these models the subduction of the NR generates a bulge of deformation that bends the overriding plate upward. We propose that this bulge is flanked by areas of gravitational relaxation and subsidence. This model is similar to analog models of the NR subduction (Hampel et al., 2004) and numerical models of seamount subduction (Ruh et al., 2016). During the MIS 13 and 9 Cerro El Huevo was located at the edge of the subsiding area leading to northward tilting of the terrace sequence. The subsequent southward migration of the

https://doi.org/10.5194/egusphere-2025-5364
Preprint. Discussion started: 18 December 2025

ridge positioned Cerro El Huevo at the hinge between uplift and subsidence, resulting in near horizontal marine terraces during MIS 7. As the ridge continued to migrate, Cerro El Huevo reached the leading flank of the uplifting bulge, causing a southwards tilt of the sequences between MIS 7 and MIS 5c. This interpretation is supported by modeled subsidence rates of ~-0.2 m/ka for MIS 13 and 11 at Cerro El Huevo, which progressively increased to 0.8 m/ka until MIS 5c (Jara-Muñoz et al., 2019). Moreover, considering the southward migration rate of 43 mm/yr for the NR over the past 5 Ma (Hampel, 2002), the observed change in tilt polarity between MIS 13 and MIS 5c would require ~20 km of southward ridge displacement (Fig. 6C). This is approximately the distance between Cerro El Huevo and the limit of the uplift bulge documented by Hsu (1992) and Macharé and Ortlieb (1992) (Fig. 4B). These results highlight the importance of accurate and precise shoreline-angle mapping for detecting subtle variations in marine terrace elevations, which are key to constrain the responsible deformation mechanisms.

2.3 Automated mapping using ICESat-2 altimetry data

The resolution of a digital topography dataset can strongly influence the accuracy of marine terrace mapping. However, the availability of high-resolution topography is scarce and limited to specific areas. Nevertheless, the satellite mission Ice, Cloud, and land Elevation Satellite-2 (ICESat-2, NASA's Earth observation program), launched in September 2018, offers open access to data with characteristics similar to high-resolution LiDAR topography (Markus et al., 2017) at global scale. The satellite carries the Advanced Topographic Laser Altimeter System (ATLAS), a photon-counting system designed to measure surface elevation with centimeter-level accuracy (Field et al., 2020). Originally developed to monitor ice sheet dynamics and sea ice, ICESat-2 also provides valuable topographic data for terrestrial and coastal environments (Abdalati et al., 2010; Jasinski et al., 2021; Markus et al., 2017). The satellite follows a near-polar, sun-synchronous orbit, enabling consistent global coverage. ICESat-2 provides a 2D high-resolution along-track sampling, with photon returns spaced approximately 20 cm, allowing for detailed bare-earth elevation profiling and making it particularly useful for analyzing geomorphic features such as marine terraces. However, the complexity of data products, structures, and the programming knowledge required for bulk download and processing makes this data difficult to access.

TerraceM-3 includes a user-friendly GUI to facilitate the selection, download, and processing of ICESat-2 data (Fig. 3, See Supplementary material Sections S3 and S4, figures S8 to S27). The download functionality of TerraceM ICESat-2 is built on python and html languages linked to MATLAB®, enabling efficient data retrieval from the Harmony online servers allowing cloud data subsets. Once downloaded, the data is processed using the built-in h5read function of MATLAB®, alongside a set of custom TerraceM scripts created to extract orbital and geolocation parameters. To extract the profiles, two ICESat-2 data products are utilized: ATL03 (geolocated photon data) and ATL08 (canopy and ground classification). ATL03 provides raw photon elevations, while ATL08 classifies photons into different surface types, enabling the isolation of ground points and the generation of bare-earth topographic profiles (See supplementary materials Section S3). Furthermore, the TerraceM ICESat-2

https://doi.org/10.5194/egusphere-2025-5364
Preprint. Discussion started: 18 December 2025

module creates lightweight structured datasets, at least ~20% of the original data size and easy to manipulate in MATLAB®, which can be helpful when data storage is limited.

Additionally, TerraceM ICESat-2 allows estimating shallow coastal bathymetry (Fig. 3), useful for extending marine terrace mapping offshore and to model the hydrodynamic parameters controlling coastal erosion at present-day. The new module uses ATL03 photon data identifying water-penetrating photons up to ~40 m depth in low turbidity conditions. Water-refraction corrections based on the method proposed by Parrish et al. (2019) and Ranndal et al. (2021) are used to account for changes in photon trajectory driven by density variations from air to water. The topographic and bathymetric analysis scripts are incorporated into TerraceM-3, including a graphical user interface (GUI) encoded in MATLAB® (TerraceM ICESat-BAT) and separate functions for customized coding outside the GUI.

One limitation of the TerraceM_ICESat-2 module arises from the predominantly N–S ground tracks of the ICESat-2 satellite. As a result, marine terraces along coastlines oriented roughly E–W are most suitable for mapping, since this geometry provides profiles perpendicular to the terrace inner edges. A further limitation is memory demand, as downloading and processing areas larger than ~40 km² may exceed the capacity of standard desktop computers (~32 GB RAM). For this reason, the tool is best applied to local areas or site-specific studies. Nevertheless, beyond the standard GUI, TerraceM_ICESat functions can be accessed individually, enabling users to develop custom scripts and adapt the processing workflows, thereby providing flexibility and overcoming memory limitations.

2.3.1 Deciphering deformation gradients along the Sahel Ridge in Algeria using ICESat-2 altimetry and automated mapping

We selected the marine terraces at Sahel Ridge, NE Algeria, which exposes a staircase sequence of more than seven levels of marine terraces and provides excellent conditions to test the TerraceM-ICESat mapping workflow. The marine terraces and rasas extend for more than 150 km between Tipaza and Algiers and comprise upper Pre- and co-Messinian and lower post-Messinian marine terraces, which ages range from Late Miocene to Late Pleistocene respectively (Authemayou et al., 2017). The marine terrace elevations reflect the deformation produced by the convergence between the African and Eurasian plates at 4 - 6 mm/yr (Nocquet and Calais, 2004), which has resulted in crustal compression since the late Miocene driving reverse faulting and folding, such as the Sahel ridge and various blind reverse faults offshore (Yelles et al., 2009; Strzerzynski et al., 2010) (Fig. 7A). This area is seismically active, characterized by historic and recent strong magnitude (Mw > 6) tsunamigenic earthquakes (Meghraoui et al., 1988; Harbi et al., 2007; Maouche et al., 2011) (Fig. 7A).

https://doi.org/10.5194/egusphere-2025-5364
Preprint. Discussion started: 18 December 2025

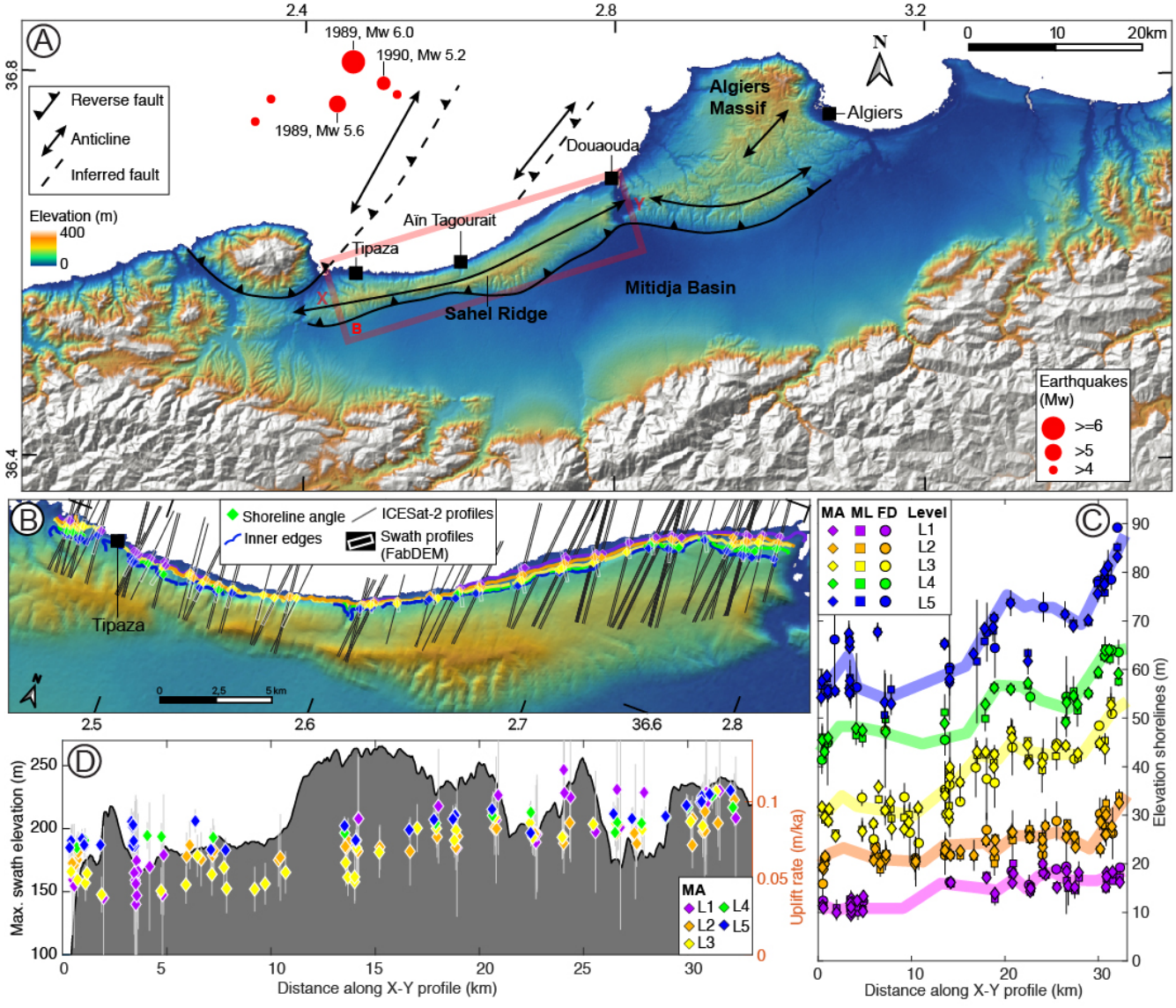

Figure 7: Tectonic setting of NE Algeria and marine terraces. A) Tectonics of the Sahel Ridge area (based on Maouche et al. 2011, Anthemayou et al., 2017). Red dots denote >Mw 4 to >=Mw 6 earthquakes. B) Marine terraces between Tipaza and Douaouda; the colored dots represent the shoreline angles mapped using ICESat-2 photon profiles (grey lines). C) Marine terrace elevations projected along the profile X-Y indicated in A. D) Uplift rates and maximum topography along the X-Y swath profile indicated in A. MA: Manually mapped shoreline angles using ICESat-2 profiles. ML: Shoreline angles mapped using machine learning and ICESat-2 profiles. FD: Manually mapped shoreline angles using 30-m resolution FABDEM topography.

We studied a 33-km-long segment of the marine terraces between the cities of Tipaza and Douaouda (Fig. 7A), an area of well-studied and dated marine terraces in E-W orientation, ensuring ICESat-2 profiles are almost perpendicular to the terraces. The marine terraces have been carved on the northern flank of the Sahel ridge (Lamothe and De, 1911; Aymé, 1952; Glangeaud,

https://doi.org/10.5194/egusphere-2025-5364
Preprint. Discussion started: 18 December 2025

1932; Saoudi, 1985). This structure has been interpreted as an anticline associated with a north-dipping blind thrust that bounds the southern edge of the Sahel ridge (Meghraoui, 1991; Maouche et al., 2011; Heddar et al., 2013). We focus on the lower (post-Messinian) marine terraces formed between MIS 11 and MIS 5e (Authemayou et al., 2017). The lowest terraces were dated using U-Th, resulting in ages between MIS 5e and the Holocene, whereas the upper terraces remain undated with inferred ages of MIS 11 and older (Authemayou et al., 2017; Maouche et al., 2011). To test the accuracy and precision of the new TerraceM ICESat-2, we mapped the post-Messinian marine terraces using three methods: manual mapping using 30 m/pixel FABDEM Forest And Buildings removed Copernicus DEM (FD) topography (Uhe et al., 2022), manual mapping (MA), and machine-learning (ML) mapping, both using ICESat-2 vegetation-filtered topographic profiles.

Our results are consistent with the marine terrace elevation estimates of Anthemayou et al. (2017) for the same area; furthermore, terrace elevations show an eastward increase comparable to that described in their study (Fig. 7C). We follow the nomenclature and chronology used by these authors, correlating level 1 with MIS 5e (120 ka), level 2 with MIS 9 (322 ka), and level 3 with MIS 11 (400 ka). From this correlation, we derive a mean uplift rate of 0.07 m/ka, close to the mean 0.06 m/ka estimated by Anthemayou et al. (2017). Assuming constant uplift, we assign levels 4 and 5 to MIS 15 and MIS 19, with ages of 615 and 775 ka respectively by assuming a constant uplift rate of 0.07 m/ka (Fig. 8A). The highstand ages and sea-level positions used in this assessment were based on the sea-level curves of Bintanja et al. (2005) and Spratt and Lisiecki (2016).

The marine terraces between Tipaza and Aïn Tagourait record a stable uplift rate of about 0.06 m/ka, gradually increasing eastwards to ~0.12 m/ka near Douaouda. The distribution of uplift rates shows some scatter; for example, near Tipaza, level 1 exhibits broad variability in urbanized areas due to anthropogenic modification of the topography. In addition, uplift rates associated with level 1 are slightly higher than those of the other levels, suggesting an uplift acceleration since MIS 5e, consistent with the observations of Anthemayou et al. (2017). Interestingly, the deformation pattern approximately mimics the maximum topography of the Sahel Ridge, indicating a possible relationship between the long-term anticlinal growth and coastal uplift.

https://doi.org/10.5194/egusphere-2025-5364
Preprint. Discussion started: 18 December 2025

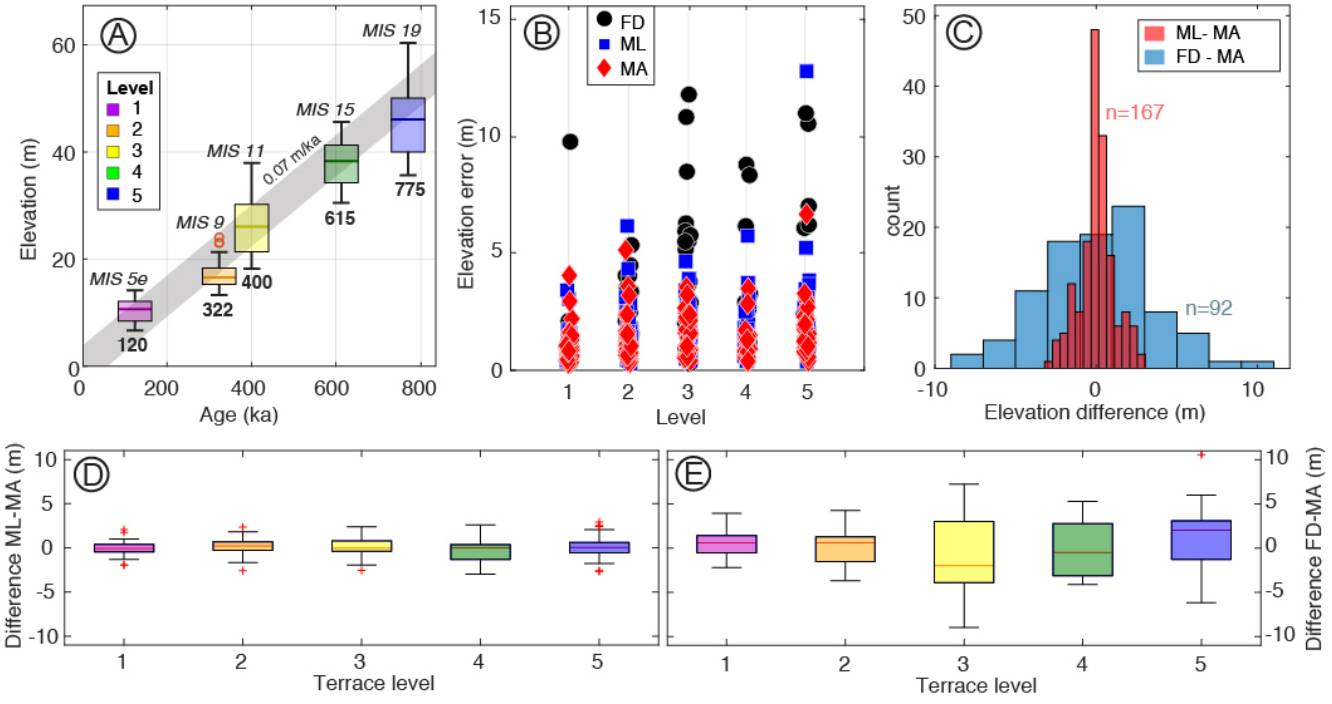

Figure 8: Statistics of different shoreline-angle mapping methods applied along the Sahel Ridge, NE Algeria. A) Shoreline-angle elevations versus marine terrace ages. Age assignments for levels 1–3 follow Anthemayou et al. (2017), while the ages of levels 4 and 5 are based on the extrapolation of uplift rate. B) Shoreline-angle elevation errors for each mapped shoreline, note the higher errors for shoreline angles mapped using FABDEM (FD). C) Distributions of elevation differences between manually (MA) and machine-learning (ML) mapped shoreline-angles using ICESat-2 profiles, and between FABDEM and ICESat-2 manual mapping (FD-MA). Notice the higher dispersion of the results based on FABDEM mapping. D) Boxplots showing the difference in elevations between machine-learning and manual mapping both using ICESat-2 profiles. E) Boxplots showing the difference in elevations between FD and MA shoreline angles.

The mapping of the Sahel Ridge terraces yielded broadly consistent results across methods, though with different levels of precision and accuracy. Elevation errors (Ze) of individual shoreline angles are larger when using FD mapping compared to MA and ML approaches using ICESat-2 profiles. This difference reflects the much higher resolution of ICESat-2 data (point spacing 10–30 cm) relative to the 30 m/px FABDEM resolution, which better captures slope gradients and allows clearer identification of paleo-cliffs. To evaluate accuracy and precision, we compared elevation differences between methods for each mapped shoreline angle. Shoreline angles obtained using FD have a lower precision (greater dispersion) than those from ICESat-2, with maximum differences of ±10 m and ±3 m, respectively (Fig. 8C–E). Comparisons between MA and ML mapping on ICESat-2 profiles reveal only minor differences between mean values (0.2 – 0.4 m), with ML values slightly underestimated. In contrast, comparisons involving MA and FD yield mean differences of up to 3 m, underscoring the lower accuracy of FD shoreline-angle mapping.

https://doi.org/10.5194/egusphere-2025-5364
Preprint. Discussion started: 18 December 2025

Our results demonstrate that the choice of a topographic dataset strongly affects both the precision and accuracy of shoreline-angle mapping. Shoreline angles derived from ICESat-2 profiles show higher precision and accuracy than those obtained from FD. The small elevation differences between machine-learning and manual mapping indicate that the performance of the machine learning approach is comparable to that of an experienced user. These findings highlight the efficiency of the TerraceM-3 mapping approach for marine terrace mapping when combined with ICESat-2 altimetry data.

3. Analysis of human-machine interactions in marine terrace mapping

It has always been a challenge to make machines replicate the qualitative aspects of the human decision process (e.g. Peterson et al., 2021). For instance, a human operator relies on sensory input, experience, and information processing to control a machine. Similarly, operators use their perception and experience to observe and interpret the results produced by the machine. These machine operations form a cycle of human-machine interactions (Farhan Hussain et al., 2023). The communication and exchange between a human and a machine are facilitated through a user interface (Georga et al., 2018). This interface enables the operator to efficiently visualize sensed quantities and input commands to control the machine. Analogous to the above relationships, TerraceM represents the machine, while the marine terrace mapping tool represents the user interface.

To study the factors controlling human–machine interaction in the classical TerraceM mapping tool, we carried out an experiment with nine geology students from the University of Potsdam, who had no previous experience with the software. They were asked to map four marine terrace profiles in a loop (Fig. 9A). Each operator performed the mapping for 25 minutes, yielding a total of 1,094 shoreline-angle measurements. The 25-minute duration was chosen to obtain enough measurements (on average ~120 per operator), while avoiding fatigue or distraction during the task.

The results show that the dispersion of shoreline-angle measurements, calculated in 2-minute time bins and expressed as the standard deviation, progressively decreased over the course of the experiment (Fig. 9B and D). This reduction in variability indicates a gradual improvement in user consistency as mapping skills developed. Likewise, the mean elevation of the mapped shoreline angles converged toward the reference elevation previously defined by an experienced interpreter (red line in Fig. 9C), demonstrating a clear learning trajectory. At the beginning of the experiment, the limited experience of participants in identifying marine terrace morphologies produced large deviations in shoreline-angle estimates, particularly in sectors where terrace boundaries were poorly defined or affected by topographic artifacts. With increasing time and feedback, however, users displayed improved recognition, resulting in more stable and accurate outputs.

https://doi.org/10.5194/egusphere-2025-5364
Preprint. Discussion started: 18 December 2025

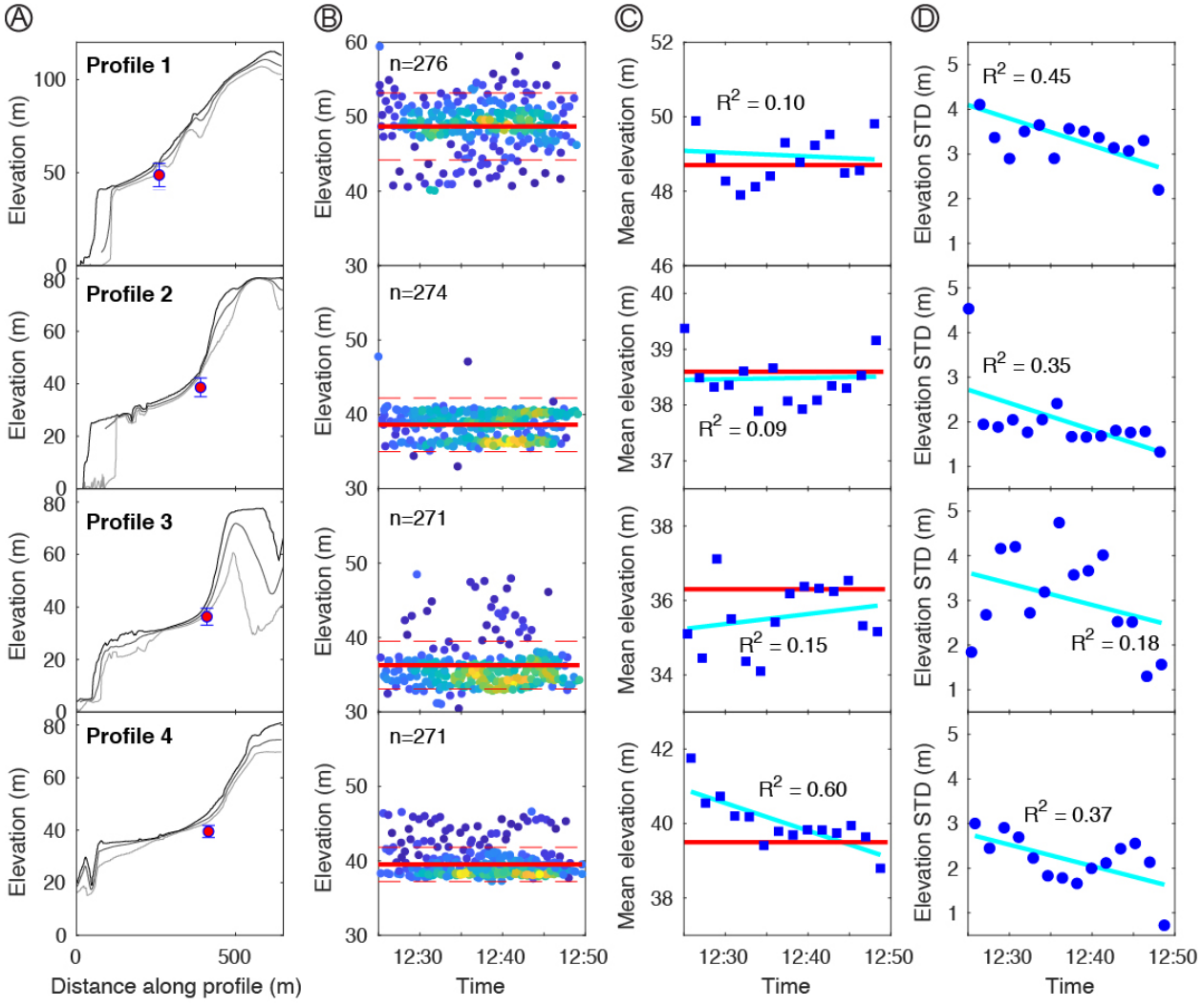

Figure 9: Shoreline-angle mapping experiment. A) Four topographic swath profiles used in the experiment. The red point is the shoreline angle mapped by an experienced user. B) Shoreline-angle elevations mapped by nine students during the experiment (n: number of measurements). C and D) Evolution of shoreline-angle mapping elevations and dispersion during the experiment, the blue squares and dots are calculated by binning measurements every two minutes. The light blue lines in C and D are linear regression with their corresponding goodness of fit (root mean squared error, R^2). Red lines in B, C and D are the shoreline-angle elevations mapped by an experienced user.

These results provide quantitative evidence of a learning curve in manual terrace mapping, in which cognitive pattern recognition and decision-making progressively align with expert-level interpretation. The observed convergence toward expert reference values highlights that terrace-mapping accuracy is not solely dependent on data quality but also on the capacity to identify subtle morphological signals through experience. Importantly, this learning process can be formalized and replicated computationally: the sequence of recognition, evaluation, and classification steps performed by trained users has been

https://doi.org/10.5194/egusphere-2025-5364
Preprint. Discussion started: 18 December 2025

translated into the machine-learning algorithms of TerraceM-3, capable of identifying shoreline angles automatically with precision comparable to that achieved by an experienced user.

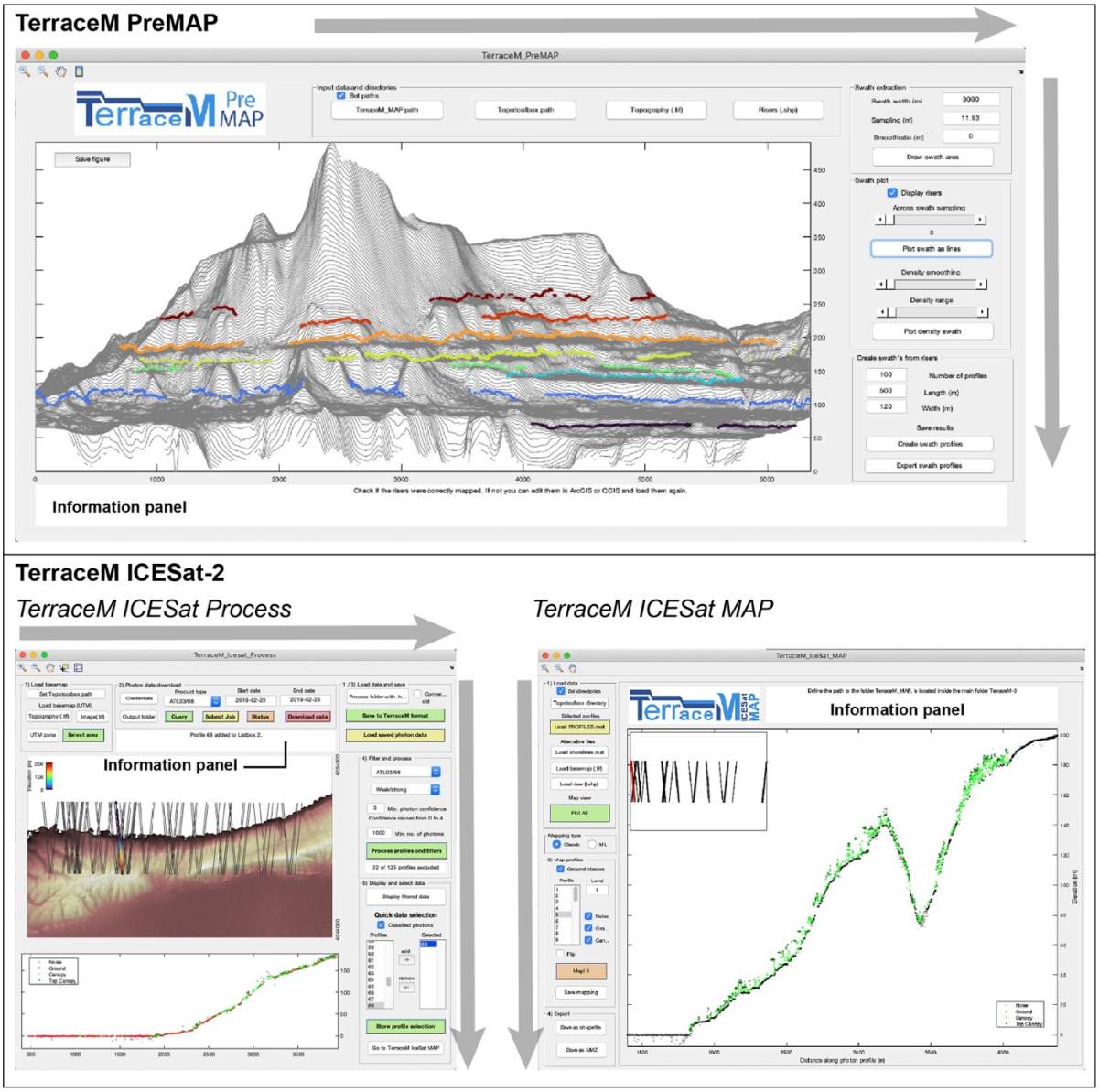

Figure 10: Graphical user interfaces of the main modules implemented in TerraceM-3. Grey arrows indicate the direction of the workflow. Information on the additional GUIs is provided in Supplementary materials, Sections S1 and S4. The software and interface shown are original work created by the authors.

https://doi.org/10.5194/egusphere-2025-5364
Preprint. Discussion started: 18 December 2025

Beyond the mapping algorithms, the interaction between the operator and TerraceM can significantly influence the results. Complex interfaces may lead to workflows that are difficult to follow and increase the likelihood of errors during analysis and processing. To minimize this, TerraceM was designed with an intuitive graphical interface and linear workflow that guides users through data loading or downloading, processing, and terrace mapping. Contextual information is dynamically displayed within dedicated panels of the GUI, assisting the operator throughout the procedure (Fig. 10). This user-centered design enhances the consistency of terrace elevations and deformation rate estimates, while providing a friendly and efficient environment that facilitates further research on marine terrace analysis and surface deformation along coastal areas.

4. Conclusions

TerraceM-3 introduces new approaches to reduce systematic and non-systematic errors in marine terrace mapping. Systematic errors associated with lateral correlation of marine terrace level and the geometry of swath profiles used for marine terrace mapping are solved using the Terrace_PreMAP tool, which provides a systematic way to cross-check and standardize marine terrace measurements. Non-systematic errors are reduced by following a machine learning approach, which allows to effectively substitute the qualitative aspect of marine terrace mapping, and associated non-systematic errors, with a tool capable of performing as reliably as a trained human user.

Finally, considering that one of the main limitations of marine terrace mapping is the scarcity of high-resolution topography, we created a new TerraceM_ICESat-2 module to download, process and analyze 2D topographic data of the ICESat-2 mission. This tool is coupled with the machine-learning mapping tool, facilitating the marine terrace mapping process. This release of TerraceM furthermore includes a Python version to map marine terraces outside the MATLAB® environment (See Supplementary material Section S5). The new additions of TerraceM-3 will expedite marine and lacustrine abrasion terrace analysis and deformation rate estimations along coastal areas ensuring methodological repeatability.

5. Code availability

The TerraceM scripts in MATLAB® language are available at Zenodo at https://zenodo.org/records/17439972 and at http://www.terracem.com

6. Author contribution

JJ-M designed the software and methodology, conducted the formal analysis, data curation, and wrote the original manuscript. JM contributed to the conceptualization and the design of the machine-learning algorithms. RF contributed to data curation for neural network training. DM contributed to the conceptualization and formal analysis. MW supported the methodology

https://doi.org/10.5194/egusphere-2025-5364
Preprint. Discussion started: 18 December 2025

development and Python programming. PW contributed to the conceptualization and formal analysis. CM contributed to conceptualization, methodology development and supervision of MW. MS participated in the conceptualization and formal analysis. All authors contributed to editing the manuscript and the revision of the final version.

7. Competing interests

The authors declare that they have no conflict of interest.

8. Acknowledgments

We gratefully acknowledge support of our Greek colleagues, Prof. Dr. Konstantinos Tsanakas, Dr. Dimitrios-Vasileios Batzakis and Diamantina Griva for their support testing the TerraceM code in the Hochschule Biberach, Germany. We also thank Dr. Simone Racano for his insights on TerraceM functionalities and suggestions. We also thank Prof. Aicha Heddar and Dr. Yahia Mohammedi for their feedback on the application of TerraceM in Algeria.

9. Financial support

This study was supported by TANTA “Earthquakes and coastal deformation in subduction zones at continental scale” grant P2022-13-001 funded by the Carl-Zeiss-Stiftung; the Millennium Nucleus CYCLO “The Seismic Cycle Along Subduction Zones” grant NC160025 funded by the Millennium Scientific Initiative (ICM) of the Chilean Government; the Chilean National Fund for Development of Science and Technology (FONDECYT) grant 1150321; and the German Science Foundation (DFG) grant STR373/41-1. The visit of the colleagues who tested TerraceM-3 was supported by KINETICS: Kithera Neotectonic analysis funded by DAAD (German Academic Exchange Service) under grant 57730124.

10. References

Abdalati, W., Zwally, H. J., Bindschadler, R., Csatho, B., Farrell, S. L., Fricker, H. A., Harding, D., Kwok, R., Lefsky, M., and Markus, T.: The ICESat-2 laser altimetry mission, Proceedings of the IEEE, 98, 735-751, 2010.

Anderson, R., Densmore, A., and Ellis, M.: The generation and degredation of marine terraces, Basin Research, 11, 7-19, 1999.

Armijo, R., Lacassin, R., Coudurier-Curveur, A., and Carrizo, D.: Coupled tectonic evolution of Andean orogeny and global climate, Earth-Science Reviews, 143, 1-35, 2015.

Armijo, R., Meyer, B., King, G., Rigo, A., and Papanastassiou, D.: Quaternary evolution of the Corinth Rift and its implications for the Late Cenozoic evolution of the Aegean, Geophysical Journal International, 126, 11-53, 1996.

Atkinson, M., Gesing, S., Montagnat, J., and Taylor, I.: Scientific worflows: Past, present and future, Future Generation Computer Systems, 216 - 227, 10.1016/j.future.2017.05.041, 2017.

Authemayou, C., Pedoja, K., Heddar, A., Molliex, S., Boudiaf, A., Ghaleb, B., Van Vliet Lanoe, B., Delcaillau, B., Djellit, H., and Yelles, K.: Coastal uplift west of Algiers (Algeria): pre-and post-Messinian sequences of marine terraces and rasas and their associated drainage pattern, International Journal of Earth Sciences, 106, 19-41, 2017.

https://doi.org/10.5194/egusphere-2025-5364
Preprint. Discussion started: 18 December 2025

Aymé, A.: Le Quaternaire littoral des environs d'Alger, Actes du Congrès Panafricain de Préhistoire, IIe session, Alger, 242-246, 1952.
Bello-González, J. P., Contreras-Reyes, E., and Arriagada, C.: Predicted path for hotspot tracks off South America since Paleocene times: Tectonic implications of ridge-trench collision along the Andean margin, Gondwana Research, 64, 216-234, 2018.
Berryman, K.: Age, height, and deformation of Holocene marine terraces at Mahia Peninsula, Hikurangi subduction margin, New Zealand, Tectonics, 12, 1347-1364, 1993.
Bintanja, R., van de Wal, R. S., and Oerlemans, J.: Modelled atmospheric temperatures and global sea levels over the past million years, Nature, 437, 125-128, 2005.
Bishop, C.: The Multi-Layer Perceptron In: Neural Networks for Pattern Recognition, 1995.
Bowles, C. J. and Cowgill, E.: Discovering marine terraces using airborne LiDAR along the Mendocino-Sonoma coast, northern California, Geosphere, 8, 386-402, 2012.
Broecker, W. S., Thurber, D. L., Goddard, J., Ku, T.-L., Matthews, R., and Mesolella, K.: Milankovitch hypothesis supported by precise dating of coral reefs and deep-sea sediments, Science, 159, 297-300, 1968.
Burbank, D. W. and Anderson, R. S.: Tectonic geomorphology, John Wiley & Sons2011.
Cerrone, C., Di Donato, V., Mazzoli, S., Robustelli, G., Soligo, M., Tuccimei, P., and Ascione, A.: Development and deformation of marine terraces: Constraints to the evolution of the Campania Plain Quaternary coastal basin (Italy), Geomorphology, 385, 107725, https://doi.org/10.1016/j.geomorph.2021.107725, 2021.
Chang, K.-t. and Tsai, B.-w.: The Effect of DEM Resolution on Slope and Aspect Mapping, Cartography and Geographic Information Systems, 18, 69-77, 10.1559/152304091783805626, 1991.
Chappell, J.: Geology of coral terraces, Huon Peninsula, New Guinea: a study of Quaternary tectonic movements and sea-level changes, Geological Society of America Bulletin, 85, 553-570, 1974.
Chiba, T., Kaneta, S.-i., and Suzuki, Y.: Red relief image map: new visualization method for three dimensional data, The international archives of the photogrammetry, remote sensing spatial information sciences, 37, 1071-1076, 2008.
Curveur, A. C.: Evolution morpho-tectonique de la marge de subduction andine au Nord Chili, Paris 7, 2012.
de Gelder, G., Husson, L., Pastier, A.-M., Fernández-Blanco, D., Pico, T., Chauveau, D., Authemayou, C., and Pedoja, K.: High interstadial sea levels over the past 420ka from the Huon Peninsula, Papua New Guinea, Communications Earth Environment, 3, 256, 2022.
DeMets, C., Gordon, R. G., Argus, D., and Stein, S.: Current plate motions, Geophysical journal international, 101, 425-478, 1990.
Duff, R. O.: Uplifted marine terraces and some other aspects of late quarternary geology in northern Taranaki, PhD, University of Otago, 1993.
Farhan Hussain, R., Mokhtari, A., Ghalambor, A., and Amini Salehi, M.: Chapter 5 - Threats and side-effects of smart solutions in O&G industry: Smartness is not necessarily smart, in: IoT for Smart Operations in the Oil and Gas Industry, edited by: Farhan Hussain, R., Mokhtari, A., Ghalambor, A., and Amini Salehi, M., Gulf Professional Publishing, 133-161, https://doi.org/10.1016/B978-0-32-391151-1.00014-9, 2023.
Fialko, Y. and Pearse, J.: Sombrero uplift above the Altiplano-Puna magma body: Evidence of a ballooning mid-crustal diapir, Science, 338, 250-252, 2012.
Field, C., Martino, A., and Ramos-Izquierdo, L.: ICESat-2/ATLAS instrument linear system impulse response, Earth Space Sci., 10504651, https://doi.org/10./essoar, 2020.
Forte, A. M. and Whipple, K. X.: The topographic analysis kit (TAK) for TopoToolbox, Earth Surface Dynamics, 7, 87-95, 2019.
Freisleben, R., Jara-Muñoz, J., Melnick, D., Martínez, J. M., and Strecker, M. R.: Marine terraces of the last interglacial period along the Pacific coast of South America (1 N–40 S), Earth System Science Data Discussions, 2020, 1-39, 2020.
Geertsma, J.: Land subsidence above compacting oil and gas reservoirs, Journal of petroleum technology, 25, 734-744, 1973.
Georga, E. I., Fotiadis, D. I., and Tigas, S. K.: 9 - Existing and Potential Applications of Glucose Prediction Models, in: Personalized Predictive Modeling in Type 1 Diabetes, edited by: Georga, E. I., Fotiadis, D. I., and Tigas, S. K., Academic Press, 201-220, https://doi.org/10.1016/B978-0-12-804831-3.00009-1, 2018.

https://doi.org/10.5194/egusphere-2025-5364
Preprint. Discussion started: 18 December 2025

Ghazleh, S. A. and Kempe, S.: Geomorphology of Lake Lisan terraces along the eastern coast of the Dead Sea, Jordan, Geomorphology, 108, 246-263, 2009.
Ghazleh, S. A. and Kempe, S.: Discovery of high-level terraces of last glacial Lake Lisan (Dead Sea) and eastern mediterranean paleoclimatic implications, Quaternary International, 604, 38-50, 2021.
Glangeaud, L.: Étude géologique de la région littorale de la province d'Alger: par Louis Glangeaud, Y. Cadoret1932.
Griggs, G. and Trenhaile, A.: Coastal cliffs and platforms, Cambridge University Press, Cambridge, UK1994.
Hampel, A.: The migration history of the Nazca Ridge along the Peruvian active margin: a re-evaluation, Earth and Planetary Science Letters, 203, 665-679, 2002.
Hampel, A., Kukowski, N., Bialas, J., Huebscher, C., and Heinbockel, R.: Ridge subduction at an erosive margin: The collision zone of the Nazca Ridge in southern Peru, Journal of Geophysical Research: Solid Earth, 109, 2004.
Hanks, T. C., Bucknam, R. C., Lajoie, K. R., and Wallace, R. E.: Modification of wave-cut and faulting-controlled landforms, Journal of Geophysical Research: Solid Earth (1978-2012), 89, 5771-5790, 1984.
Harbi, A., Maouche, S., Vaccari, F., Aoudia, A., Oussadou, F., Panza, G., and Benouar, D.: Seismicity, seismic input and site effects in the Sahel—Algiers region (North Algeria), Soil Dynamics and Earthquake Engineering, 27, 427-447, 2007.
Heddar, A., Authemayou, C., Djellit, H., Yelles, A., Déverchère, J., Gharbi, S., Boudiaf, A., and Lanoe, B. V. V.: Preliminary results of a paleoseismological analysis along the Sahel fault (Algeria): New evidence for historical seismic events, Quaternary International, 302, 210-223, 2013.
Henriquet, M., Avouac, J.-P., and Bills, B. G.: Crustal rheology of southern Tibet constrained from lake-induced viscoelastic deformation, Earth and Planetary Science Letters, 506, 308-322, 2019.
Holzer, T. L. and Johnson, A. I.: Land subsidence caused by ground water withdrawal in urban areas, GeoJournal, 11, 245-255, 1985.
Hsu, J.: Emerged quaternary marine terraces in southern Peru: Sea level changes and continental margin tectonics over the subducting Nazca Ridge, Cornell Univ., Ithaca, NY (USA), 1988.
Hsu, J. T.: Quaternary uplift of the Peruvian coast related to the subduction of the Nazca Ridge: 13.5 to 15.6 degrees south latitude, Quaternary International, 15-16, 87-97, 1992.
Jara-Muñoz, J. and Melnick, D. J. Q. R.: Unraveling sea-level variations and tectonic uplift in wave-built marine terraces, Santa María Island, Chile, 83, 216-228, 2015.
Jara-Muñoz, J., Melnick, D., and Strecker, M. R.: TerraceM: A MATLAB(R) tool to analyze marine and lacustrine terraces using high-resolution topography, Geosphere, 12, 20, 10.1130/ges01208.1, 2016.
Jara-Muñoz, J., Melnick, D., Pedoja, K., and Strecker, M. R.: TerraceM-2: A Matlab® interface for mapping and modeling marine and lacustrine terraces, Frontiers in Earth Science, 7, 255, 2019.
Jara-Muñoz, J., Agnon, A., Fohlmeister, J., Tomás, S., Mey, J., Frank, N., Schröder, B., Schröder-Ritzrau, A., Garcin, Y., and Darvasi, Y.: Unveiling the Transition From Paleolake Lisan to Dead Sea Through the Analysis of Lake Paleoshorelines and Radiometric Dating of Fossil Stromatolites, Geochemistry, Geophysics, Geosystems, 25, e2024GC011541, 2024.
Jasinski, M., Stoll, J., Hancock, D., Robbins, J., Nattala, J., Moriso, J., Jones, B., Ondrusek, M., Pavelsky, T., and Parrish, C.: ATLAS/ICESat-2 L3B mean inland surface water data, NASA National Snow
Ice Data Center Distributed Active Archive Center data set, ATL22. 001, 2021.
Johannsen, G.: Human-machine interaction, Control Systems, Robotics and Automation, 21, 132-162, 2009.
Johnson, D.: Problems of terrace correlation, Bulletin of the Geological Society of America, 55, 793-818, 1944.
Kaizuka, S., Matsuda, T., Nogami, M., and Yonekura, N.: Quaternary tectonic and recent seismic crustal movements in the arauco peninsula and its environs, central chile, Geographical reports of Tokyo Metropolitan University, 8, 1-49, 1973.
Kavzoglu, T.: Increasing the accuracy of neural network classification using refined training data, Environmental Modelling Software, 24, 850-858, 2009.
Krishnan, S., Crosby, C., Nandigam, V., Phan, M., Cowart, C., Baru, C., and Arrowsmith, R.: OpenTopography: a services oriented architecture for community access to LIDAR topography, Proceedings of the 2nd international conference on computing for Geospatial Research & Applications, 1-8,
Lajoie, K. R.: Coastal tectonics, Active Tectonics, 95-124, 1986.
Lambeck, K.: Glacial crustal rebound, sea levels and shorelines, Encyclopaedia of Ocean Sciences, 2, 1157-1167, 2001.
Lamothe, d. and De, L.: Les anciennes lignes de rivage du Sahel d'Alger et d'une partie de la côte Algérienne, Societe geologique de France1911.

https://doi.org/10.5194/egusphere-2025-5364
Preprint. Discussion started: 18 December 2025

Macharé, J. and Ortlieb, L.: Plio-Quaternary vertical motions and the subduction of the Nazca Ridge, central coast of Peru, Tectonophysics, 205, 97-108, 1992.
Maouche, S., Meghraoui, M., Morhange, C., Belabbes, S., Bouhadad, Y., and Haddoum, H.: Active coastal thrusting and folding, and uplift rate of the Sahel Anticline and Zemmouri earthquake area (Tell Atlas, Algeria), Tectonophysics, 509, 69-80, 2011.
Markus, T., Neumann, T., Martino, A., Abdalati, W., Brunt, K., Csatho, B., Farrell, S., Fricker, H., Gardner, A., and Harding, D.: The Ice, Cloud, and land Elevation Satellite-2 (ICESat-2): science requirements, concept, and implementation, Remote sensing of environment, 190, 260-273, 2017.
Matsu'ura, T.: Late Quaternary uplift rate inferred from marine terraces, Muroto Peninsula, southwest Japan: Forearc deformation in an oblique subduction zone, Geomorphology, 234, 133-150, 2015.
Matsu'ura, T., Komatsubara, J., and Wu, C.: Accurate determination of the Pleistocene uplift rate of the NE Japan forearc from the buried MIS 5e marine terrace shoreline angle, Quaternary Sci Rev, 212, 45-68, 2019.
Matsu'ura, T., Kimura, H., Komatsubara, J., Goto, N., Yanagida, M., Ichikawa, K., and Furusawa, A.: Late Quaternary uplift rate inferred from marine terraces, Shimokita Peninsula, northeastern Japan: A preliminary investigation of the buried shoreline angle, Geomorphology, 209, 1-17, 2014.
Meghraoui, M.: Blind reverse faulting system associated with the Mont Chenoua-Tipaza earthquake of 29 October 1989 (north-central Algeria), Terra nova, 3, 84-92, 1991.
Meghraoui, M., Philip, H., Albarede, F., and Cisternas, A.: Trench investigations through the trace of the 1980 El Asnam thrust fault: Evidence for paleoseismicity, Bulletin of the Seismological Society of America, 78, 979-999, 1988.
Melnick, D.: Rise of the central Andean coast by earthquakes straddling the Moho, Nature Geoscience, 9, 401-407, 2016.
Melnick, D., Yıldırım, C., Hillemann, C., Garcin, Y., Ciner, A., Pérez-Gussinyé, M., and Strecker, M. R.: Slip along the Sultanhanı Fault in Central Anatolia from deformed Pleistocene shorelines of palaeo-lake Konya and implications for seismic hazards in low-strain regions, Geophysical Journal International, 209, 1431-1454, 2017.
Mitusio, T.: The middle terrace problems in Shikoku, Japan, Kochi University0913-1302, 187-202, 1989.
Neuenschwander, A. and Pitts, K.: The ATL08 land and vegetation product for the ICESat-2 Mission, Remote sensing of environment, 221, 247-259, 2019.
Nocquet, J.-M. and Calais, E.: Geodetic measurements of crustal deformation in the Western Mediterranean and Europe, Pure and applied geophysics, 161, 661-681, 2004.
Norabuena, E., Leffler-Griffin, L., Mao, A., Dixon, T., Stein, S., Sacks, I. S., Ocola, L., and Ellis, M.: Space geodetic observations of Nazca-South America convergence across the central Andes, Science, 279, 358-362, 1998.
Ortlieb, L. and Macharé, J.: Geocronologia y morfoestratigrafia de terrazas marinas del Pleistoceno superior: el caso de San Juan-Marcona, Peru, Boletin de la Sociedad Geologica del Peru, 81, 87-106, 1990.
Palamara, D. R., Dickson, M. E., and Kennedy, D. M.: Defining shore platform boundaries using airborne laser scan data: a preliminary investigation, Earth Surface Processes and Landforms, 32, 945-953, 10.1002/esp.1485, 2007.
Pan, L., Powell, E. M., Latychev, K., Mitrovica, J. X., Creveling, J. R., Gomez, N., Hoggard, M. J., and Clark, P. U.: Rapid postglacial rebound amplifies global sea level rise following West Antarctic Ice Sheet collapse, Science Advances, 7, eabf7787, 2021.
Parrish, C. E., Magruder, L. A., Neuenschwander, A. L., Forfinski-Sarkozi, N., Alonzo, M., and Jasinski, M.: Validation of ICESat-2 ATLAS bathymetry and analysis of ATLAS's bathymetric mapping performance, Remote sensing of environment, 11, 1634, 2019.
Pedoja, K., Husson, L., Regard, V., Cobbold, P. R., Ostanciaux, E., Johnson, M. E., Kershaw, S., Saillard, M., Martinod, J., and Furgerot, L.: Relative sea-level fall since the last interglacial stage: Are coasts uplifting worldwide?, Earth-Science Reviews, 108, 1-15, 2011.
Peterson, J. C., Bourgin, D. D., Agrawal, M., Reichman, D., and Griffiths, T. L.: Using large-scale experiments and machine learning to discover theories of human decision-making, Science, 372, 1209-1214, 10.1126/science.abe2629, 2021.
Randdal, H., Sigaard Christiansen, P., Kliving, P., Baltazar Andersen, O., and Nielsen, K.: Evaluation of a Statistical Approach for Extracting Shallow Water Bathymetry Signals from ICESat-2 ATL03 Photon Data, 10.3390/rs13173548, 2021.

https://doi.org/10.5194/egusphere-2025-5364
Preprint. Discussion started: 18 December 2025

Regard, V., Saillard, M., Martinod, J., Audin, L., Carretier, S., Pedoja, K., Riquelme, R., Paredes, P., and Hérail, G.: Renewed uplift of the Central Andes Forearc revealed by coastal evolution during the Quaternary, Earth and Planetary Science Letters, 297, 199-210, 2010.

Roberts, G. P., Meschis, M., Houghton, S., Underwood, C., and Briant, R. M.: The implications of revised Quaternary palaeoshoreline chronologies for the rates of active extension and uplift in the upper plate of subduction zones, Quaternary Sci Rev, 78, 169-187, 10.1016/j.quascirev.2013.08.006, 2013.

Rosenbloom, N. A. and Anderson, R. S.: Hillslope and channel evolution in a marine terraced landscape, Santa Cruz, California, Journal of Geophysical Research: Solid Earth, 99, 14013-14029, 1994.

Ruh, J. B., Sallarès, V., Ranero, C. R., and Gerya, T.: Crustal deformation dynamics and stress evolution during seamount subduction: High-resolution 3-D numerical modeling, Journal of Geophysical Research: Solid Earth, 121, 6880-6902, 2016.

Saillard, M., Hall, S., Audin, L., Farber, D., Regard, V., and Hérail, G.: Andean coastal uplift and active tectonics in southern Peru: 10Be surface exposure dating of differentially uplifted marine terrace sequences (San Juan de Marcona,~ 15.4 S), Geomorphology, 128, 178-190, 2011.

Saoudi, N.-E.: Pliocène et Pléistocène inférieur et moyen du Sahel occidental d'Alger, Bulletin de liaison-Association sénégalaise pour l'étude du quaternaire de l'ouest africain, 67-70, 1985.

Sato, T. and Matsu'Ura, M.: Cyclic crustal movement, steady uplift of marine terraces, and evolution of the island arc-trench system in southwest Japan, Geophysical Journal International, 111, 617-629, 1992.

Schleidgen, S., Friedrich, O., Gerlek, S., Assadi, G., and Seifert, J.: The concept of “interaction” in debates on human–machine interaction, Humanities and Social Sciences Communications, 10, 551, 10.1057/s41599-023-02060-8, 2023.

Shirzaei, M., Freymueller, J., Törnqvist, T. E., Galloway, D. L., Dura, T., and Minderhoud, P. S.: Measuring, modelling and projecting coastal land subsidence, Nature Reviews Earth Environment, 2, 40-58, 2021.

Simms, A. R., Rouby, H., and Lambeck, K.: Marine terraces and rates of vertical tectonic motion: The importance of glacio-isostatic adjustment along the Pacific coast of central North America, Bulletin, 128, 81-93, 2016.

Singer, B. S., Le Mével, H., Licciardi, J. M., Córdova, L., Tikoff, B., Garibaldi, N., Andersen, N. L., Diefenbach, A. K., and Feigl, K. L.: Geomorphic expression of rapid Holocene silicic magma reservoir growth beneath Laguna del Maule, Chile, Science Advances, 4, eaat1513, 2018.

Spratt, R. M. and Lisiecki, L. E.: A Late Pleistocene sea level stack, Climate of the Past, 12, 1079-1092, 2016.

Stephenson, W.: Rock coasts, Coastal environments global change, 356-379, 2015.

Strzerzynski, P., Déverchère, J., Cattaneo, A., Domzig, A., Yelles, K., Mercier de Lépinay, B., Babonneau, N., and Boudiaf, A.: Tectonic inheritance and Pliocene-Pleistocene inversion of the Algerian margin around Algiers: Insights from multibeam and seismic reflection data, Tectonics, 29, 2010.

Tang, Y., Kurths, J., Lin, W., Ott, E., and Kocarev, L.: Introduction to Focus Issue: When machine learning meets complex systems: Networks, chaos, and nonlinear dynamics, Chaos: An Interdisciplinary Journal of Nonlinear Science, 30, 063151, 10.1063/5.0016505, 2020.

Trenhaile, A., Pepper, D., Trenhaile, R., and Dalimonte, M.: Stacks and notches at Hopewell Rocks, New Brunswick, Canada, Earth Surface Processes and Landforms, 23, 975-988, 1998.

Uhe, P., Hawker, L., Paulo, L., Sosa, J., Sampson, C., and Neal, J.: FABDEM-A 30m global map of elevation with forests and buildings removed, EGU General Assembly Conference Abstracts, EGU22-8994,

Wang, S.-C.: Artificial Neural Network, in: Interdisciplinary Computing in Java Programming, edited by: Wang, S.-C., Springer US, Boston, MA, 81-100, 10.1007/978-1-4615-0377-4_5, 2003.

Wu, Y.-c. and Feng, J.-w.: Development and Application of Artificial Neural Network, Wireless Personal Communications, 102, 1645-1656, 10.1007/s11277-017-5224-x, 2018.

Yelles, A., Domzig, A., Déverchère, J., Bracène, R., Mercier de Lépinay, B., Strzerzynski, P., Bertrand, G., Boudiaf, A., Winter, T., and Kherroubi, A.: Evidence for large active fault offshore west Algiers, Algeria, and seismotectonic implications, Tectonophysics, 475, 98-116, 2009.